Theoretical and Applied Mechanics Letters xxx (xxxx) xxx

Contents lists available at ScienceDirect

Theoretical and Applied Mechanics Letters

journal homepage: www.elsevier.com/locate/taml

Letter

Wall-resolved large-eddy simulation of turbulent channel flows with rough walls

Shilong Li[a,b], Xiaolei Yang[a,b,*], Guodong Jin[a,b], Guowei He[a,b]

[a] The State Key Laboratory of Nonlinear Mechanics, Institute of Mechanics, Chinese Academy of Sciences, Beijing 100190, China
[b] School of Engineering Sciences, University of Chinese Academy of Sciences, Beijing 100049, China

ARTICLE INFO

Article history:
Received 12 December 2020
Revised 18 December 2020
Accepted 22 December 2020
Available online xxx

Keywords:
Rough wall turbulence
Curvilinear immersed boundary method
Wall-resolved large eddy simulation

ABSTRACT

Turbulent flows over rough surfaces widely exist in nature and industry. Investigating its mechanism is of theoretical and practical significance. In this work we simulate the turbulent channel flow with rough walls using large-eddy simulation with rough elements resolved using the curvilinear immersed boundary method and compare the results obtained in this work with those in the paper by Yuan and Piomelli (*J. Fluid Mech.*, vol. 760, pp. R1, 2014), where the volume of fluid method was employed for modeling rough elements. The mean streamwise velocity profiles predicted by the two methods agree well with each other. Differences in Reynolds stresses and dispersive stresses are observed, which are attributed to the different approaches in dealing with the complex geometry of the rough surface.

© 2021 Published by Elsevier Ltd on behalf of The Chinese Society of Theoretical and Applied Mechanics.
This is an open access article under the CC BY-NC-ND license
(http://creativecommons.org/licenses/by-nc-nd/4.0/)

1. Introduction

Turbulent flows in nature and industry often happen with rough surfaces [1]. An abundant literature is available for turbulent flow in channels with rough elements of various shapes [1–3], for instance rectangular bar, cube and semi-sphere. Ignoring the specific geometry of rough elements, the simplest way for modeling rough walls is using the logarithmic law [1,4], which can predict the downward shift of the streamwise velocity profile and the increase of skin friction coefficient due to surface roughness. The logarithmic law can be expressed as follows:

$$U^+\left(y^+\right) = \frac{1}{\kappa}\log\left((y-d)^+\right) + B - \Delta U^+\left(k_s^+\right), \tag{1}$$

where the superscript '+' indicates the scaling in viscous units, i.e. $y^+ = yu_\tau/\nu$ and $U^+ = U/u_\tau$ ($u_\tau = \sqrt{\tau_w/\rho}$ is the friction velocity, where τ_w and ρ are the total wall stress, which includes form stress from the roughness elements and viscous stress, and fluid density, respectively), ν is the kinematic viscosity, $\kappa \approx 0.4$ is the Kármán constant, $5 < B < 5.5$ is a universal constant, ΔU^+ is the roughness function defining the roughness-dependent velocity defect, k_s is the "equivalent" sand roughness, and zero-plane displacement d is the effective elevation of the boundary layer, which depends on type of roughness. Using the roughness length k_0 as the characteristic length scale, the logarithmic law for rough wall can be rewritten in the following form,

$$U^+ = \frac{1}{\kappa}\log\left(y/k_0\right), \tag{2}$$

where $k_0 = 0.033k_s$. The logarithmic law can predict the collective impacts of roughness elements on the outer flow, but it cannot predict the heterogeneous flow structures near the rough surface. Advanced models have been developed in the literature to account for such heterogeneous effects. For instance, Yang et al. [5] developed an analytical model for the turbulent boundary layer flow over rectangular-prism roughness elements based on large-eddy simulation results.

It has been shown in the literature that the flow near the rough surface may have significant effects on related flow dynamics [1,6]. For instance, Vowinckel et al. [7] showed that the flow below the roughness crest can affect the evolution of mobile granular beds. Giometto et al. [8] demonstrated that it can affect the spatial characteristics of the mean flow over a realistic urban surface. Besides the mean shear in the vertical direction, wakes behind rough elements dominate the flow dynamics near the rough surface. It was shown in [6] that wakes behind roughness elements depend on the geometry of the roughness. And these wakes may have significant impacts on the dispersive stresses (form-induced stresses) in the lower part of the roughness sublayer, which describe the spatial heterogeneity of the time-averaged flow [9,10]. The dependence of the roughness function on different roughness topography was dis-

* Corresponding author.
E-mail address: xyang@imech.ac.cn (X. Yang).

https://doi.org/10.1016/j.taml.2021.100228
2095-0349/© 2021 Published by Elsevier Ltd on behalf of The Chinese Society of Theoretical and Applied Mechanics. This is an open access article under the CC BY-NC-ND license (http://creativecommons.org/licenses/by-nc-nd/4.0/)

Please cite this article as: S. Li, X. Yang, G. Jin et al., Wall-resolved large-eddy simulation of turbulent channel flows with rough walls, Theoretical and Applied Mechanics Letters, https://doi.org/10.1016/j.taml.2021.100228

cussed by Wu et al. [11]. The topographical effects of roughness on turbulence statistics in roughness sublayer were discussed by Yuan and Jouybari [12]. In [10], Yuan and Piomelli systematically studied the form drag, dispersive stresses, TKE budgets and WKE (wake kinetic energy) budgets in channel flows with rough walls. In [13], Wu and Piomelli examined the combined effects of roughness and adverse pressure gradient on separated turbulent boundary layers [13].

Because of the important effects of wakes behind rough elements on the turbulent flow over rough wall turbulence, it is critical to directly resolve the flow at the scale of roughness elements. Different numerical methods have been employed in the literature for rough-resolved simulations, e.g. methods based on body-fitted grids [14,15], lattice Boltzmann method [16] and immersed boundary (IB) method [10]. Methods based on body-fitted grids and lattice Boltzmann method are often limited to relatively regular rough surfaces, such as square bars [14], gradual roughness elements [15] and hemisphere [11,16]. IB methods, on the other hand, can simulate flows with arbitrarily complex boundaries [17–20]. In the IB method employed in [10,21,22], the volume-of-fluid (VOF) approach is used to represent the complex geometry of the rough wall by specifying the velocity at the grid cell cut by the rough surface based on the volume fraction of fluid. The VOF method is relatively easy to implement. One disadvantage of the VOF method is that it is less accurate in representing the geometry of the rough surface as the location and orientation of the surface is not explicitly accounted for in the cells cut by the surface. In this work, we employ the sharp interface, curvilinear immersed boundary method (CURVIB) [23], which explicitly takes into account the geometry information of the rough surface when reconstructing the velocity at grid nodes near the boundary, to simulate turbulent flows over rough surfaces and compare the obtained results with those presented in [10]. Specifically, we simulate the fully developed turbulent flow with rough elements, which are generated in the same way as in [10] (the case R2 in [10]).

In the rest of the paper, we first introduce the employed numerical method including the flow solver and the CURVIB method, and the computational setup in Section 2 and Section 3, respectively. Then, we present the simulation results and compare them with the results from Yuan and Piomelli [10] in Section 4. At last, in Section 5 we draw conclusions from this work.

2. Numerical methods

2.1. Flow solver

In this work the LES module of the virtual flow simulator (VFS-Wind) [24,25] code is employed for simulating the flow over rough wall. It has been successfully applied to different environmental and energy problems [25–29]. The governing equations are the three-dimensional, unsteady, filtered continuity and Navier-Stokes equations shown as follows:

$$\frac{\partial u_i}{\partial x_i} = 0, \tag{3}$$

$$\frac{\partial u_i}{\partial t} + \frac{\partial u_i u_j}{\partial x_j} = -\frac{\partial p}{\partial x_i} + \frac{\partial}{\partial x_j}\left(\nu \frac{\partial u_i}{\partial x_j} - \tau_{ij}\right), \tag{4}$$

where $x_i (i = 1, 2, 3)$ are the Cartesian coordinates, u_i is the ith component of the velocity vector in Cartesian coordinates, ν is the kinematic viscosity, p is the pressure, and τ_{ij} represents the anisotropic part of the subgrid-scale stress tensor, which is modeled by the dynamic subgrid-scale model [30]. The governing equations are discretized in space using a second-order accurate central differencing scheme, and integrated in time using the fractional step method [23]. An algebraic multigrid acceleration along with a GMRES solver is used to solve the pressure Poisson equation. A matrix-free Newton–Krylov method is used for solving the discretized momentum equations.

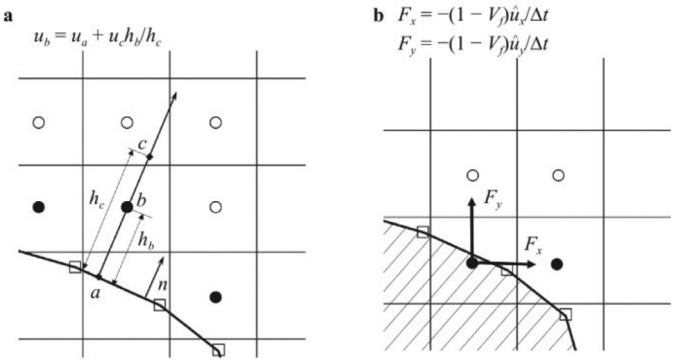

Fig. 1. Different treatment of rough surfaces for (a) the CURVIB method, where u_a, u_b and u_c are the velocities at point a, b and c, respectively, and h_b and h_c are the length of segment ab and ac and (b) the VOF method, where F_x and F_y are the x and y components of the forcing term $\mathbf{F}$.

2.2. Immersed boundary method

The CURVIB [23] is employed in VFS-Wind to represent complex boundaries. As show in Fig. 1a, the Cartesian grid nodes are classified as fluid nodes located in the fluid and solid nodes located in the solid. The fluid nodes with at least one neighbor in the solid are marked as IB nodes (e.g. point b in Fig. 1a). In CURVIB, the velocity at IB nodes are constructed in the wall normal direction using the velocity at the boundary (point a in Fig. 1a) and velocity in the fluid (point c in Fig. 1a), where the velocity at point c is interpolated from the surrounding fluid nodes. For wall-resolved large-eddy simulation, in which point b is located in the viscous sublayer, the linear interpolation is employed. For wall-modeled large-eddy simulation, in which the viscous sublayer is not resolved by the grid, the velocity at point b is constructed using a wall model [5,24,31,32].

The simulation results of this work will be compared with results from Yuan and Piomelli [10] by Yuan and Piomelli, which are computed using the VOF method. Here we briefly describe the VOF method employed in [10]. In this method, the flow is first solved without the forcing to obtain the preliminary velocity $\hat{\mathbf{u}}$. Then the forcing terms applied to the grid cells cut by the boundary (field circles shown in Fig. 1b) are calculated by $\mathbf{F} = -(1 - V_f)\frac{\hat{\mathbf{u}}}{\Delta t}$, where V_f is the volume fraction of fluid, and Δt is the time step. This forcing term is determined by requiring that the velocity at the cells cut by boundary is equal to $V_f\hat{\mathbf{u}}$. With this forcing term, the governing equations are solved to obtain the velocity for this time step.

3. Computational setup

We simulate the turbulent channel flow over rough wall, which has been carried out earlier by Yuan and Piomelli [10]. The Reynolds number based on the channel height h and the bulk velocity U_b is $Re = 12207$. A schematic of the rough surface employed in this work is shown in Fig. 2, which is generated using the virtual sandgrain model proposed in [21]. In this approach, the bottom surface is partitioned into square tiles of size $2r \times 2r$ with each tile containing a randomly rotated ellipsoid with semiaxes r, $1.4r$ and $2r$ and its center located at $z_0 = -0.5r$ (as shown in Fig. 2). In the simulated case, the value of r is set as $r/h = 0.07$ corresponding to the fully rough regime (the R2 case in reference [10]), where h is the height of the channel. It is noticed that the "equivalent" sand

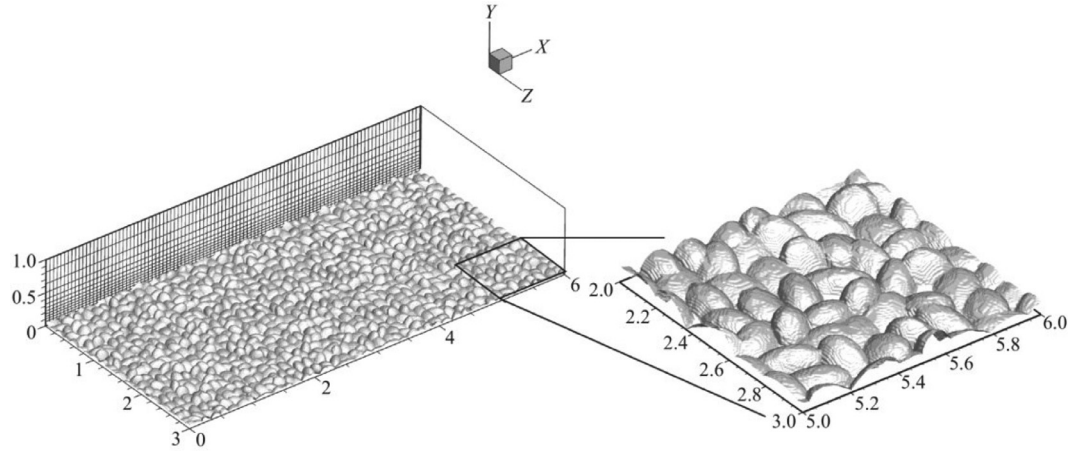

Fig. 2. Schematic of the computational domain and the rough surface. On the slice, every tenth grid line is displayed.

roughness $k_s = r$ is known a priori given by the virtual sandgrain model [21].

The size of the computational domain is $6h \times h \times 3h$ in x, y and z direction, respectively, which has been shown sufficient to accommodate the largest turbulent structures for a smooth-wall channel flow [10]. The free-slip boundary condition is applied at the top boundary, while at the bottom wall with rough surface, the no-slip condition is employed. Periodic boundary conditions are imposed in the streamwise and spanwise directions (x and z, respectively). The computational domain is discretized using $1024 \times 128 \times 512$ grid nodes in the x, y and z directions, respectively (uniform grids in the x and z directions), with each square tile resolved by 24 grid nodes in the horizontal directions. The grid is refined near the wall in the y direction (as shown in Fig. 2), with the first off grid spacing $\Delta y/h = 3.75 \times 10^{-3}$ and 28 nodes allocated below the roughness crest. The size of time step is $\Delta t U_b/h = 2 \times 10^{-3}$. In the present case, the flow is driven by a mean pressure gradient, which is computed by maintaining a constant mass flux. The flow is first simulated for about 20 flow-throughs to achieve a fully developed state. Then the turbulence statistics are obtained by continuing the simulation for about 30.7 flow-throughs.

A space-time double-averaging approach [9] is used to analyze turbulence statistics. In this approach, a flow quantity θ can be decomposed into space-time average, $\langle\overline{(\theta)}\rangle$, the spatial variation of the temporal average, $\widetilde{(\theta)}$, and the turbulent fluctuation θ' as follows:

$$\theta(x,y,z,t) = \langle\overline{\theta}\rangle(y) + \widetilde{\theta}(x,y,z) + \theta'(x,y,z,t), \tag{5}$$

in which, $\bar{\cdot}$ denotes temporal averaging, $\langle\cdot\rangle$ denotes the spatial average over the fluid nodes in the horizontal directions. Another superficial averaging $\langle\cdot\rangle_s$ can also be carried out in the whole horizontal plane without considering whether the grid node is located in the fluid or in the solid [33].

4. Results

In this section, we present our the simulation results and compare them with Yuan and Piomelli's [10]. In this work, we fix the bulk velocity in the simulation and compute the friction velocity based on the forces exerted on the rough elements. The Reynolds number based on the channel lengths (h) and friction velocity u_τ is $Re_\tau = 1050$ for the present case, close to $Re_\tau = 1000$ of reference [10], with the roughness heights in wall unit $k_s^+ = 75$ and $k_s^+ = 72$ respectively for our case and that in [10]. We first show the instantaneous flow field in Fig. 3. As seen, the wake behind each rough element and the heterogeneous distribution of the streamwise velocity are well captured by the employed method. In Fig. 4 we

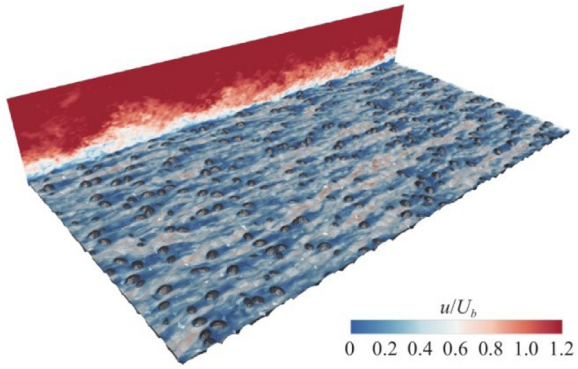

Fig. 3. Contour of instantaneous streamwise velocity on the x-y plane located at $x/h = 0$ and the x-z plane located at $y/h = 0.07$, respectively. Where U is the instantaneous streamwise velocity.

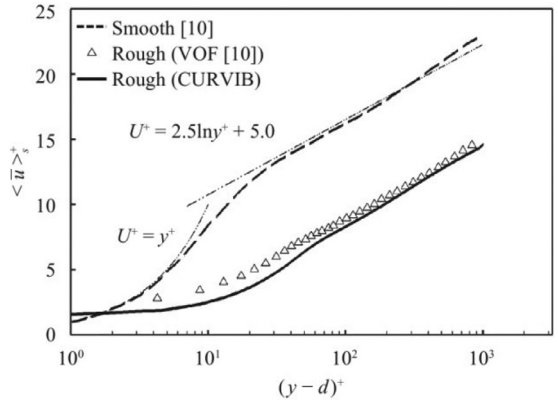

Fig. 4. Comparison of the vertical profiles of the streamwise velocity computed using the CURVIB method with that computed using the VOF method [10] and that of of smooth channel.

show the temporally and horizontally averaged streamwise velocity profile in wall units. It is seen that the velocity profile computed from this work agrees well with that in [10] with the normalized velocity defect in the logarithmic region approximately 7.8. Differences are observed in the roughness sublayer (i.e. $y < 2k_s$ with its physical meaning discussed later), where the mean streamwise velocity profile predicted in this work is slightly lower than that from [10]. This is probably because of the different treatments of rough elements in the two methods that the no-slip boundary condition

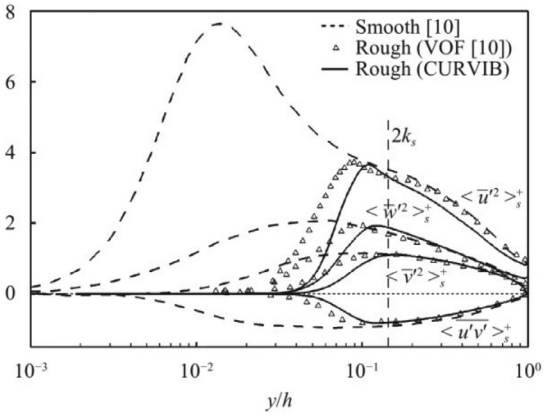

Fig. 5. Comparison of the Reynolds stresses computed using the CURVIB method with those computed using the VOF method and those of smooth channel. The Reynolds stresses are normalized using u_τ^2.

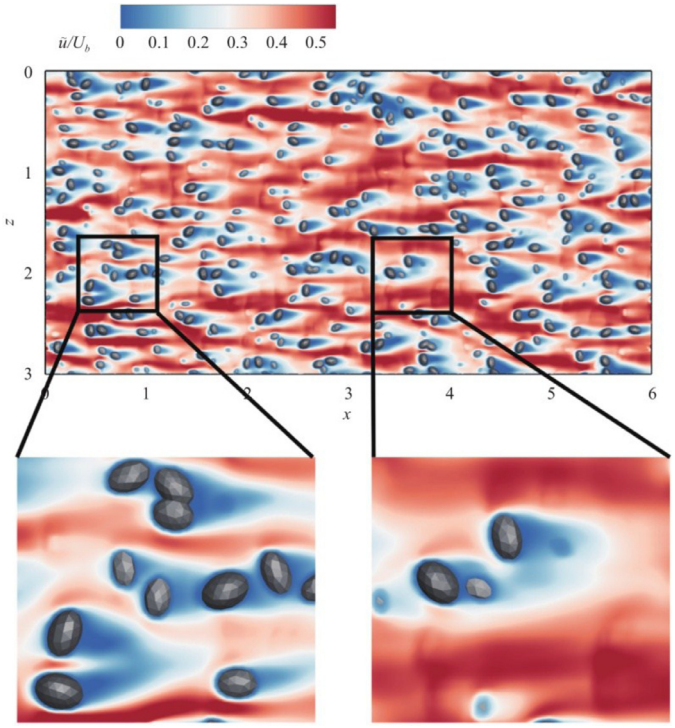

Fig. 6. Contours of time-averaged streamwise velocity on the $x-z$ plane located at $(y-d)^+ = 10$ with two regions of the slice is zoomed in with one containing more rough elements cut by the slice than the other.

is explicitly imposed in the CURVIB method but not in the VOF method.

In Fig. 5 we compare the Reynolds stresses normalized by u_τ^2 as a function of y/h computed from this work, with those from the smooth wall case ($Re_\tau = 1000$) and the same rough wall case in [10]. As seen, different terms of the Reynolds stresses are similar with each other in the outer layer down to the edge of roughness sublayer located at $y \approx 2k_s$ for different cases. This indicates that the friction velocity properly scales turbulence in the outer layer even for cases of different wall roughness. When compared with the results from the smooth wall case, it is observed that the peaks of Reynolds stresses are shifted outward and siginificantly damped in the region close to the rough surface, where the viscous sublayer and the buffer layers are destructed for rough wall turbulence in the fully rough regime. Compared with Yuan and Piomelli's results [10], the locations of peaks of the Reynolds stresses are slightly farther from the wall with the magnitudes of the Reynolds stresses damped more faster as moving from peak locations to the wall.

After showing the Reynolds stresses, here we examine the spatial heterogeneity of the flow field. We first show the time-averaged streamwise velocity was not uniform on the $x-z$ plane located at $(y-d)^+ = 10$ as in Fig. 6. As seen, the spatial distribution of the streamwise velocity is highly variable due to the rough surface formed by random rotated ellipsoids. These observed spatial heterogeneity results in the dispersive stresses[34]. Taking the dispersive shear stress as an example, it appears in the temporally and horizontally averaged momentum equation as follows:

$$-\frac{\partial\langle\bar{p}\rangle_s}{\partial x}+\nu\frac{\partial^2\langle\bar{u}\rangle_s}{\partial y^2}-\frac{\partial\langle\overline{u'v'}\rangle_s}{\partial y}-\frac{\partial\langle\tilde{u}\tilde{v}\rangle_s}{\partial y}-\left\langle\frac{\partial\tilde{p}}{\partial x}\right\rangle_s+\nu\langle\nabla^2\tilde{u}\rangle_s=0, \tag{6}$$

where $\langle\tilde{u}\tilde{v}\rangle_s$ is the dispersive shear stress. We compare the dispersive stresses computed in this work with those in [10] in Fig. 7. The physical meaning of the roughness sublayers is shown clearly in Fig. 7 that it is the region with a significant amount of dispersive stresses with its top boundary located approximately at $2k_s$. As seen in Fig. 6, the peak of the streamwise components $\langle\tilde{u}^2\rangle_s^+$ is significantly higher than that from Yuan and Piomelli [10]. The spanwise component $\langle\tilde{v}^2\rangle_s^+$ and the wall normal component $\langle\tilde{w}^2\rangle_s^+$, on the other hand, are lower than those from Yuan and Piomelli [10]. The peak of the magnitude of the dispersive shear stress $\left|\langle\tilde{u}\tilde{v}\rangle_s^+\right|$ is approximately two times smaller than that from reference [10]. These observations indicate that the flow is more heterogeneous in the streamwise direction as compared with the other two directions. Wakes behind rough elements are the main component contributing to the flow heterogeneity. High heterogeneity in the streamwise direction probably means the wakes predicted by the CURVIB method are stronger than those from the VOF method em-

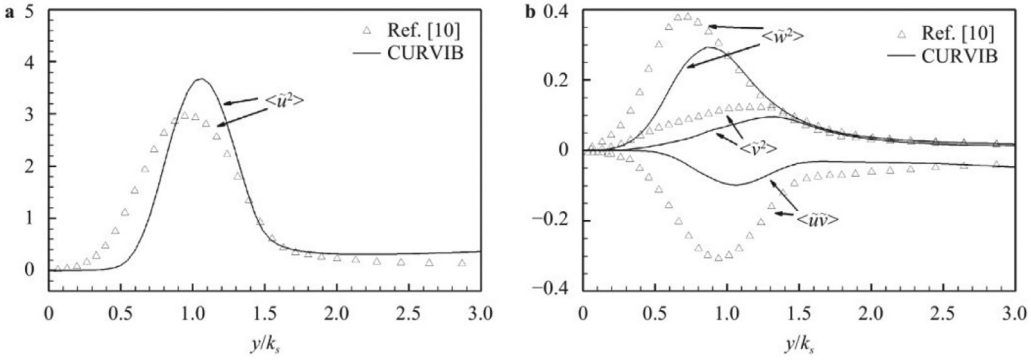

Fig. 7. Comparison of the dispersive stresses computed using the CURVIB method with those computed using the VOF method [10] for (a) the streamwise component and (b) other components. The dispersive stresses are normalized using u_τ^2.

ployed in [10]. It is also noticed that the locations of the peaks of the dispersive stresses are farther away from the wall as compared with the predictions from Yuan and Piomelli [10], which is similar to that observed in Reynolds stresses.

5. Conclusions

In this work, we carry out LES of turbulent channel flow over rough wall with the rough surface represented using the sharp interface CURVIB method. In the simulated case, the "equivalent" sand roughness is the same as that in the work by Yuan and Piomelli [10], in which the roughness elements were modeled using the VOF method. The simulation results from this work are compared with those from Yuan and Piomelli [10]. For the normal Reynolds stresses $\langle \overline{u'^2} \rangle$, $\langle \overline{v'^2} \rangle$, $\langle \overline{w'^2} \rangle$, the predictions from this work are similar to [10] in the outer region, while they are smaller than those from Yuan and Piomelli [10] in the rough wall region. For the dispersive stress, the peak of the streamwise component $\langle \tilde{u}^2 \rangle$ computed from this work is higher than that from Yuan and Piomelli [10], while the vertical and spanwise components $\langle \tilde{v}^2 \rangle$ and $\langle \tilde{w}^2 \rangle$ and the magnitude of the dispersive shear stress are lower than those from Yuan and Piomelli [10].

The differences observed between the predictions of this work and those in [10] can be explained by the different treatments of roughness elements. In the VOF method employed in [10], the velocity at those cells cut by the boundary is specified based on the volume fraction of fluid, while in the CURVIB method [10], the velocity at the IB node is reconstructed by directly satisfying the boundary conditions at the surface of the rough element. This difference probably results in larger form drag and stronger wakes behind rough elements, causing differences in the predictions of Reynolds stresses and dispersive stresses.

Declaration of Competing Interest

The authors declare that they have no known competing financial interests or personal relationships that could have appeared to influence the work reported in this paper.

Acknowledgment

This work was supported by the NSFC Basic Science Center Program for "Multiscale Problems in Nonlinear Mechanics" (No. 11988102) and the NSFC Program (No. 11772337), the Science Challenge Program (No. TZ2016001), the Strategic Priority Research Program, Chinese Academy of Sciences (CAS) (No. XDB22040104), the Key Research Program of Frontier Sciences, CAS (No. QYZDJ-SSW-SYS002) and the CAS Center for Excellence in Complex System Mechanics. We are grateful to Junlin Yuan for providing us their simulation data in [10] and her helpful suggestions.

References

[1] J. Jimenez, Turbulent flows over rough walls, Annu. Rev. Fluid Mech. 36 (1) (2004) 173–196.
[2] M. Raupach, A.S. Thom, Turbulence in and above plant canopies, Annu. Rev. Fluid Mech. 13 (1) (1981) 97–129.
[3] M. Raupach, R. Antonia, S. Rajagopalan, Rough-wall turbulent boundary layers(1991).
[4] S.B. Pope, Turbulent flows, 2001.
[5] X.I. Yang, J. Sadique, R. Mittal, C. Meneveau, Exponential roughness layer and analytical model for turbulent boundary layer flow over rectangular-prism roughness elements, J. Fluid Mech. 789 (2016) 127–165.
[6] O. Coceal, T. Thomas, I. Castro, S. Belcher, Mean flow and turbulence statistics over groups of urban-like cubical obstacles, Bound. Layer Meteorol. 121 (3) (2006) 491–519.
[7] B. Vowinckel, V. Nikora, T. Kempe, J. Fröhlich, Momentum balance in flows over mobile granular beds: application of double-averaging methodology to DNS data, J. Hydraul. Res. 55 (2) (2017) 190–207.
[8] M. Giometto, A. Christen, C. Meneveau, J. Fang, M. Krafczyk, M. Parlange, Spatial characteristics of roughness sublayer mean flow and turbulence over a realistic urban surface, Bound. Layer Meteorol. 160 (3) (2016) 425–452.
[9] E. Mignot, E. Barthélemy, D. Hurther, Double-averaging analysis and local flow characterization of near-bed turbulence in gravel-bed channel flows, J. Fluid Mech. 618 (2009) 279–303.
[10] J. Yuan, U. Piomelli, Roughness effects on the Reynolds stress budgets in near-wall turbulence, J. Fluid Mech. 760 (2014) R1.
[11] S. Wu, K.T. Christensen, C. Pantano, A study of wall shear stress in turbulent channel flow with hemispherical roughness, J. Fluid Mech. 885 (2020).
[12] J. Yuan, M.A. Jouybari, Topographical effects of roughness on turbulence statistics in roughness sublayer, Phys. Rev. Fluids 3 (11) (2018) 114603.
[13] W. Wu, U. Piomelli, Effects of surface roughness on a separating turbulent boundary layer, J. Fluid Mech. 841 (2018) 552.
[14] S. Leonardi, P. Orlandi, R. Smalley, L. Djenidi, R. Antonia, Direct numerical simulations of turbulent channel flow with transverse square bars on one wall, J. Fluid Mech. 491 (2003) 229.
[15] M. MacDonald, N. Hutchins, D. Chung, Roughness effects in turbulent forced convection, J. Fluid Mech. 861 (2019) 138–162.
[16] Y. Kuwata, Y. Kawaguchi, Direct numerical simulation of turbulence over resolved and modeled rough walls with irregularly distributed roughness, Int. J. Heat Fluid Flow 77 (2019) 1–18.
[17] F. Sotiropoulos, X. Yang, Immersed boundary methods for simulating fluid–structure interaction, Prog. Aerosp. Sci. 65 (2014) 1–21.
[18] X. Yang, X. Zhang, Z. Li, G.-W. He, A smoothing technique for discrete delta functions with application to immersed boundary method in moving boundary simulations, J. Comput. Phys. 228 (20) (2009) 7821–7836.
[19] S. Wang, X. Zhang, An immersed boundary method based on discrete stream function formulation for two- and three-dimensional incompressible flows, J. Comput. Phys. 230 (9) (2011) 3479–3499.
[20] W.-X. Huang, F.-B. Tian, Recent trends and progress in the immersed boundary method, Proc. Inst. Mech. Eng. Part C J. Mech. Eng. Sci. 233 (23-24) (2019) 7617–7636.
[21] A. Scotti, Direct numerical simulation of turbulent channel flows with boundary roughened with virtual sandpaper, Phys. Fluids 18 (3) (2006).
[22] P. Berghout, X. Zhu, D. Chung, R. Verzicco, R.J. Stevens, D. Lohse, Direct numerical simulations of Taylor–Couette turbulence: The effects of sand grain roughness, J. Fluid Mech. 361 (2019) 260–286.
[23] L. Ge, F. Sotiropoulos, A numerical method for solving the 3D unsteady incompressible Navier-Stokes equations in curvilinear domains with complex immersed boundaries, J. Comput. Phys. 225 (2) (2007) 1782–1809.
[24] X. Yang, F. Sotiropoulos, R.J. Conzemius, J.N. Wachtler, M.B. Strong, Large-eddy simulation of turbulent flow past wind turbines/farms: the virtual wind simulator (VWiS), Wind Energy 18 (12) (2015) 2025–2045.
[25] A. Calderer, X. Yang, D. Angelidis, A. Khosronejad, T. Le, S. Kang, A. Gilmanov, L. Ge, I. Borazjani, Virtual flow simulator, Technical Report, University of Minnesota, 2015.
[26] S. Kang, X. Yang, F. Sotiropoulos, On the onset of wake meandering for an axial flow turbine in a turbulent open channel flow, J. Fluid Mech. 744 (2014) 376–403.
[27] X. Yang, A. Khosronejad, F. Sotiropoulos, Large-eddy simulation of a hydrokinetic turbine mounted on an erodible bed, Renew. Energy 113 (2017) 1419–1433.
[28] S. Kang, A. Lightbody, C. Hill, F. Sotiropoulos, High-resolution numerical simulation of turbulence in natural waterways, Adv. Water Resour. 34 (1) (2011) 98–113.
[29] A. Khosronejad, S. Kang, F. Sotiropoulos, Experimental and computational investigation of local scour around bridge piers, Adv. Water Resour. 37 (2012) 73–85.
[30] M. Germano, U. Piomelli, P. Moin, W.H. Cabot, A dynamic subgrid-scale eddy viscosity model, Phys. Fluids A Fluid Dyn. 3 (7) (1991) 1760–1765.
[31] B. Shi, X. Yang, G. Jin, G. He, S. Wang, Wall-modeling for large-eddy simulation of flows around an axisymmetric body using the diffuse-interface immersed boundary method, Appl. Math. Mech. 40 (3) (2019) 305–320.
[32] S. Kang, An improved near-wall modeling for large-eddy simulation using immersed boundary methods, Int. J. Numer. Methods Fluids 78 (2) (2015) 76–88.
[33] V. Nikora, I. McEwan, S. McLean, S. Coleman, D. Pokrajac, R. Walters, Double-averaging concept for rough-bed open-channel and overland flows: theoretical background, J. Hydraul. Eng. 133 (8) (2007) 873–883.
[34] V. Nikora, D. Goring, I. McEwan, G. Griffiths, Spatially averaged open-channel flow over rough bed, J. Hydraul. Eng. 127 (2) (2001) 123–133.